Thermoelectric power of charge-neutral $Nd_{1-2x}Ca_xM_xBa_2Cu_3O_{7-\delta}$ (M=Th and Pr): Evidence for different types of localization

S. R. Ghorbani, M. Andersson, and Ö. Rapp
Solid State Physics, Department of Microelectronics and Information Technology, KTH-229, Stockholm-Kista, SE 164 40, Sweden
(Received 3 April 2002; published 27 September 2002)

The superconducting T_c of $Nd_{1-2x}Ca_xM_xBa_2Cu_3O_{7-\delta}$ (M=Th or Pr) is strongly depressed with increasing doping concentration in spite of the fact that these dopings are nominally charge neutral for small x. We have inquired into the reasons for this behavior by studies of the thermoelectric power S in sintered samples with x up to 0.1 and for temperatures from T_c up to room temperature. $S(x,T)$ was analyzed in terms of two different semiempirical models, which assume the existence of a narrow electron band. In both models and for both dopings the bands broaden with increasing x and the tendency for localization increases. For Ca-Th doping this can be explained by weak electronic disorder. For Ca-Pr doping, the increase of electronic disorder is weaker, and the results indicate that charge localization in addition is important.

DOI: 10.1103/PhysRevB.66.104519 PACS number(s): 74.62.Dh, 72.15.Jf, 74.25.Fy, 74.72.Bk

I. INTRODUCTION

The thermoelectric power (S) is highly sensitive to details of the electrical transport mechanism, and measurements of S appear to be a fruitful way of understanding the nature of the carriers and charge transport in high-T_c superconductors and related compounds. This is reflected in a large number of investigations of different alloy systems, such as $La_{2-x}Sr_xCuO_4$,[1,2] Y-123,[3–10] Bi-based materials,[11–14] and Tl- and Hg-based compounds.[15–18] These studies have revealed trends for the magnitude of S and for the temperature and doping concentration dependence. For instance, one important result is the useful empirical relation between the magnitude of S at room temperature and the hole concentration p in the planes.[15] Furthermore, for semiconducting or insulating materials with low hole concentration, S is positive and large, and decreases with increasing p. For metallic samples, on the other hand, S is small and has a characteristic behavior for both underdoped and optimally doped samples at temperatures above the superconducting transition temperature T_c. In these materials S first rises with increasing temperature towards a maximum at T_{max} and then decreases almost linearly up to at least room temperature. Both S and T_{max} decrease with increasing p in this region. For overdoped samples with larger p, S is negative. Variations in the temperature dependence of S can also be a simple way to distinguish plane and chain contributions to the transport properties.[8–10,15]

An interesting type of doping in 123 compounds is charge-neutral substitution on the Y site. The parabolic variation of T_c with varying charge concentration is suppressed in this case, and T_c varies linearly with doping concentration. In spite of the preserved structure and small changes in lattice parameters, the effect on T_c of such dopings can be remarkably strong. One example is $Nd_{1-2x}Ca_xM_xBa_2Cu_3O_{7-\delta}$ where $-dT_c/dx$ is in the region around 200 K for M=Pr or Th.[19,20] Charge-neutral dopings and a Pr 4+ valence at low doping concentrations were supported by results from neutron diffraction, e.g., the concentration dependence of the Cu-plane distance, in addition to the linear depression of T_c. Yet there are several distinct differences between Ca-Pr and Ca-Th doping. The concentration dependences of some bond valence sums (BVS) are different, indicating small differences in charge transfers,[19,20] and the muon spin relaxation rates also show different concentration dependences.[21] Furthermore, the normal-state electrical resistivity ρ increases strongly with Ca-Th doping, suggesting a disorder-induced depression of T_c, while ρ increases slowly with Ca-Pr doping, in spite of the similarly depressed T_c.[22] These observations are not well understood.

The starting point for the present paper is the question whether the thermoelectric power can contribute to understanding similarities and differences between these charge-neutral dopings. S as a function of T was measured for samples of $Nd_{1-2x}Ca_xM_xBa_2Cu_3O_{7-\delta}$ (M=Pr,Th) and analyzed in two different semiempirical two-band models. Localization increases for both dopings as evidenced in one model by the displacement of the Fermi energy towards the localized part of the band and in the other model by the decrease of the ratio of the conductivity bandwidth to the total bandwidth. For Ca-Th doping the results reinforce the picture of a disorder-driven localization, while for Ca-Pr this effect is weaker and charge localization appears to give an important contribution.

II. SAMPLE PREPARATION AND EXPERIMENTAL DETAILS

Samples of $Nd_{1-2x}Ca_xPr_xBa_2Cu_3O_{7-\delta}$ with x=0, 0.025, 0.05, and 0.10 were prepared by standard solid-state methods. Starting materials were high-purity Nd_2O_3, $BaCO_3$, CuO, $CaCO_3$, and Pr_6O_{11}. The samples were pressed into pellets and calcined in air at 900, 920, and 920 °C, respectively, with intermediate grindings. Annealing was then performed in flowing oxygen at 460 °C for 3 days, and the temperature was finally decreased to room temperature at a slow rate of 12 °C/h. For the $Nd_{1-2x}Ca_xTh_xBa_2Cu_3O_{7-\delta}$ series, samples with x=0, 0.015, 0.03, 0.05, and 0.1 were previously prepared in a similar fashion.[20] After reannealing at 460 °C for 3 days followed by a similar slow cooling, these

samples were used for the present measurements of the thermopower.

Neutron and x-ray diffraction have been made previously on the present Ca-Th samples and on similar Ca-Pr-doped samples.[19,20] In particular, Rietveld refinements of the neutron diffraction data confirmed that the doping elements entered fully the Nd sites. We performed x-ray powder diffraction on the presently made Ca-Pr-doped samples to check the phase purity. In a sensitive Guinier-Hägg focusing camera using Cu $K\alpha$ radiation with Si as internal standard, and with the photographs evaluated in a microdensitometer system,[23] no impurity reflections were observed and all lines could be indexed in the orthorhombic space group (*Pmmm*). Similar results were obtained previously for the Ca-Th-doped samples, except at $x=0.1$, where a few weak impurity lines were observed.[20] This indicates that the solubility limit for Ca-Th doping in the orthorhombic phase of Nd-123 is somewhat below $x=0.1$. This will also be apparent in the deviating trends of some properties at this concentration as discussed below.

As a further sample characterization, T_c was measured resistively for the samples. The results were similar to previous findings.[22] The transition widths ΔT_c estimated from 90%–10% of the resistance drops were narrow for sintered samples, with values below 3 K for all Nd(CaPr) samples and for Nd(CaTh) up to $x=0.03$. At $x=0.1$ in the latter series, ΔT_c was 10.5 K, indicating that the solubility in the orthorhombic phase had been reached. T_c was found to decrease linearly with doping concentration for all Ca-Pr-doped samples and up to $x=0.05$ for Ca-Th doping as expected. The depression rates were $-dT_c/dx=170$ and 230 K for Ca-Pr and Ca-Th doping, respectively, also in fair agreement with previous results.[22]

Thermoelectric power measurements were made in a temperature interval up to room temperature on bars cut from the sintered pellets. Dimensions were typically $0.5\times2.5\times11$ mm^3. Small reversible temperature gradients up to 1.5 K were used in these measurements.

III. RESULTS AND ANALYSES

A. Experimental results

Results for the temperature dependence of the thermoelectric power are shown in Fig. 1(a) for Ca-Pr-doped samples and in Fig. 1(b) for Ca-Th-doped samples. S is positive in the whole temperature range for both sample series and increases with increasing dopant concentration with an exception only at $x=0.1$ in the Ca-Th series, where, as mentioned, the solubility limit has been reached. At high temperature, S follows an almost linear temperature dependence. For decreasing temperature, S has a broad maximum slightly above the superconducting T_c and decreases strongly as T_c is approached. The chain contribution to S has a positive slope, while the plane contribution typically has a negative slope.[8–10,15] Our results hence indicate that holes in the planes give the dominating contribution to the thermopower. The curves through data in Fig. 1 exemplify fits to one of the models used to analyze S, which will be described below.

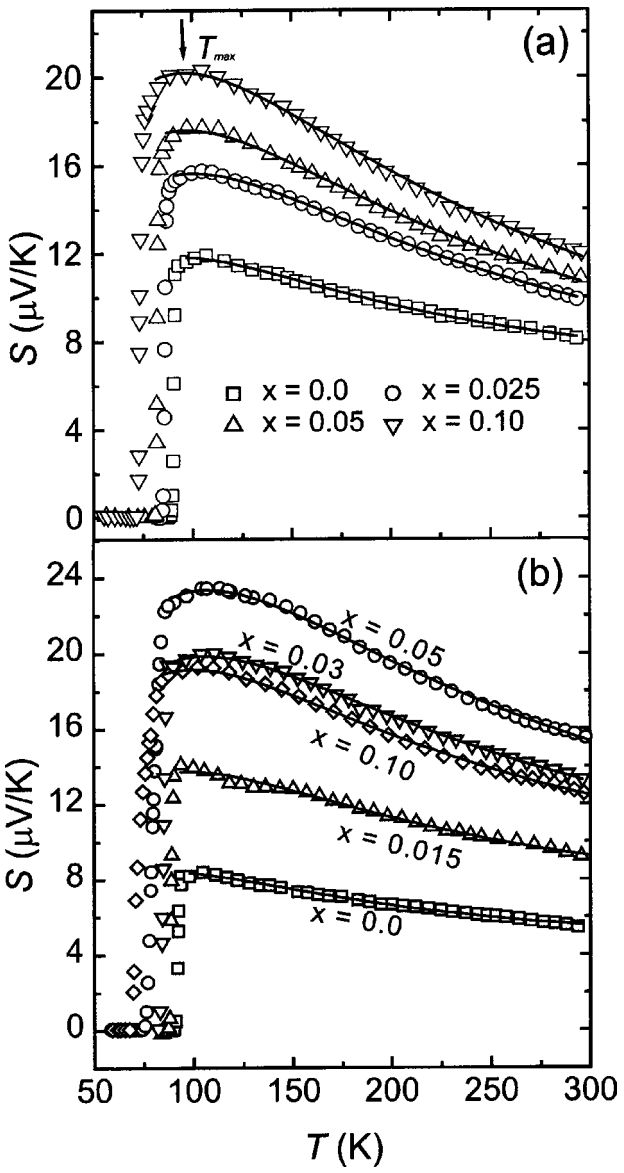

FIG. 1. Thermoelectric power S for (a) $Nd_{1-2x}Ca_xPr_xBa_2Cu_3O_{7-\delta}$ and (b) $Nd_{1-2x}Ca_xTh_xBa_2Cu_3O_{7-\delta}$ samples. The curves are fits to the model of Eq. (1). Here T_{max} is the temperature at the maximum of $S(T)$ as shown by an arrow for one sample.

Some general features of $S(T)$ can be noted prior to analyses of the models. The doping concentration dependence of S at 290 K is compared in Fig. 2 for Ca-Pr and Ca-Th dopings. In the orthorhombic phase S increases strongly for Ca-Th doping, while for Ca-Pr doping there is only a moderate increase up to $x=0.1$. According to the general trends for S outlined in the Introduction, one may conclude that there is a more pronounced weakening of the metallic state for Ca-Th doping than for Ca-Pr doping. For comparison, data for Nd-123 with a single dopant of either Ca (Ref. 24) or Pr (Ref. 25) have been included in Fig. 2. In the former case, one expects addition of holes and improved metallic properties, similar to observed resistive properties of Sm-123 doped with Ca only.[26] The concentration dependence of $S(x)$ is in agreement with this interpretation. For

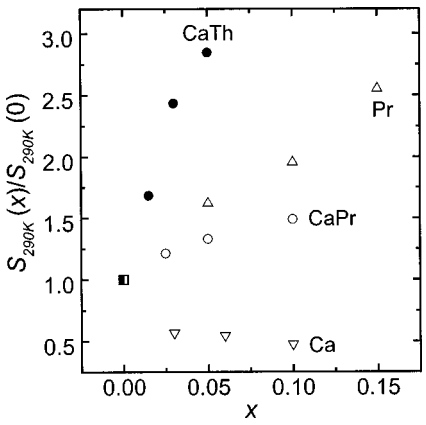

FIG. 2. Relative concentration dependence of $S(290\ \mathrm{K})$. Present data with x defined as in Fig. 1 are shown by circles. For comparison, data from Ref. 24 for $Nd_{1-x}Ca_xBa_2Cu_3O_{7-\delta}$ and from Ref. 25 for $Nd_{1-x}Pr_xBa_2Cu_3O_{7-\delta}$ are also shown.

doping with Pr only, a somewhat stronger increase of S_{290} is observed relative to the charge-neutral Ca-Pr doping, which is in qualitative agreement with the expected destruction of holes by Pr^{4+}.

Another characteristic feature of the observations is the variation with doping of the temperature $T_{\max}$ at the maximum of $S(T)$. The relative concentration dependence of $T_{\max}$ is shown in Fig. 3 for the same alloys as in Fig. 2. A datum at $x=0.015$ for Ca-Th has been omitted from the figure since in this case data were scattered in the region of the maximum in $S(T)$ and a determination of $T_{\max}$ was uncertain. The overall features of Figs. 2 and 3 are similar, reflecting a trend of weakening metallic state for Pr and Ca-Th dopings and a more pronounced effect for Ca-Th doping than for Ca-Pr doping. Dopings with only Ca indicate improved metallic properties.

Published results in other high-T_c systems display similar trends. In Bi-2212 (Ref. 27) and in T1-2212 doped with Y on a Ca site,[28] $T_{\max}$ was found to increase with doping, and this trend was stronger in the T1-based system, which showed a much stronger increase of the resistivity with doping than the Bi-based samples.[29] In Bi-2212 samples of varying oxygen

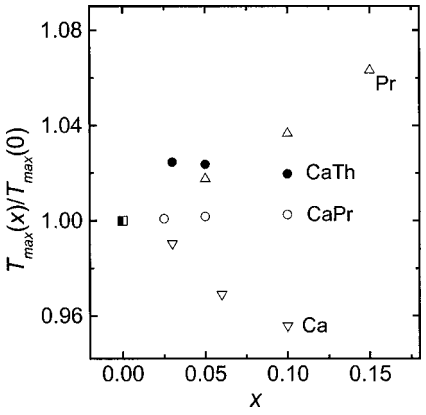

FIG. 3. Relative concentration dependence of $T_{\max}$. Circles: Present codoped samples. Open triangles: Data from Refs. 24 and 25.

concentration, an increase of the resistivity was observed, concomitant with a decrease of T_c and an increase of $T_{\max}$.[30]

B. Semiempirical models for *S*

Two models for the thermoelectric power will be used to analyze the results, both of which are based on the assumption of a narrow band for the charge carriers. Forro *et al.* suggested[30] a two-band model with an additional linear temperature term for analyzing the thermoelectric power in the temperature range above T_c (here called model 1). This expression has the following form:

$$S(T)=\frac{AT}{B^2+T^2}+\gamma T,$$
$$A=2|\varepsilon_0-\varepsilon_F|/|e|,$$
$$B^2=3[(\varepsilon_0-\varepsilon_F)^2+\Gamma^2]/\pi^2k_B^2. \tag{1}$$

The first term, as proposed by Gotwick *et al.*[31] for analyses of thermoelectric power data for $CeNi_x$ samples, is a superposition of a broad and a narrow band. The narrow band has width Γ and is positioned with its peak at ε_0 close to the Fermi energy ε_F. The second term of S is the normal band contribution. Three fitting parameters are used in this model, A, B, and γ, from which the bandwidth and distance between the narrow band peak and ε_F can be calculated.

In the phenomenological model by Gasumyants *et al.*[32] it is similarly assumed that the Fermi energy is located inside a narrow energy interval within which the density of states is larger than beyond this interval. Approximate analytical expressions were derived for the temperature dependence of the transport coefficients, and results for $S(T)$ were obtained in terms of the energy bandwidth for the density of states, w_D, the band filling fraction F—i.e., the electron concentration divided by the number of states in the band—and the bandwidth w_σ of the effective conductivity $\sigma(\varepsilon)$ (model 2). S is thus expressed in the form

$$S=S(w_D,w_\sigma,F,T) \tag{2}$$

for each sample. Equation (2) is given in the Appendix.

Both these models thus employ three free parameters to describe the fairly smooth functions $S=S(T)$ for each sample. It is therefore not surprising that in all cases the observations can be well described. The curves in Figs. 1(a) and 1(b) illustrate the fits to model 1. Typical errors in the fitting procedures are nevertheless small, of order 1% or below, and illustrate that the analyses are quite sensitive to small changes particularly in $\varepsilon_0-\varepsilon_F$ and in Γ. For model 2, the fits were indistinguishable from those in Fig. 1, and the sensitivity to variations in the fitting parameters was similarly strong, with estimated errors usually below 0.5%. In the next subsections the results for Ca-Pr and Ca-Th will be described in terms of these models.

C. Results in model 1

Γ and $\varepsilon_0-\varepsilon_F$ in Eq. (1) were calculated from the parameters A and B obtained from the analyses of $S(x,T)$. The

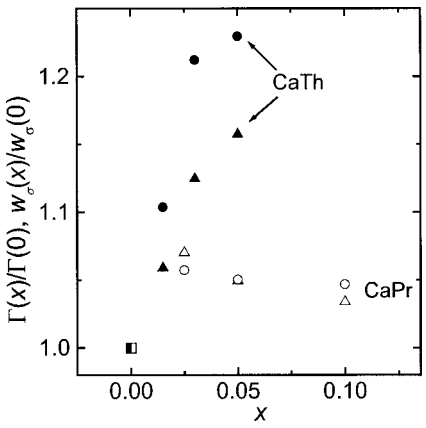

FIG. 4. Relative concentration dependence of the bandwidths Γ from model 1 and w_σ from model 2 for $Nd_{1-2x}Ca_xM_xBa_2Cu_3O_{7-\delta}$. Solid symbols: M=Th. Open symbols: M=Pr. Triangles: $w_\sigma(x)$. Circles: $\Gamma(x)$.

bandwidth Γ was found to be of the order of 15 meV. For Ca-Pr doping Γ was within 14.6 ± 0.5 meV for all samples, while for Ca-Th doping a trend of increasing Γ with x is apparent in the data up to $x=0.05$ as illustrated in Fig. 4. At $x=0.1$, at the solid solubility limit, a low value of $\Gamma(x)/\Gamma(0)=1.13$ was found (not shown in Fig. 4).

Compared with the magnitude of Γ, the variation of $\varepsilon_0-\varepsilon_F$ with doping is small. As illustrated in Fig. 5, $|\varepsilon_0-\varepsilon_F|$ increases more strongly for Ca-Th doping than for Ca-Pr. These results suggest that the Fermi energy approaches the tail of the band, diminishing the number of free charge carriers, and furthermore that this tendency for localization is somewhat stronger for Ca-Th than for Ca-Pr, in qualitative agreement with previously discussed observations.

It was found recently that the parameter γ of Eq. (1) varied with hole concentration p in a parabolic way for Nd-123 doped with either Ca or Pr.[25] The hole concentration was determined from the universal relation between p and S at 290 K.[15] The maximum of this parabola was close to the charge concentration corresponding to the maximum superconducting T_c, with p increasing for Ca doping and decreasing for Pr doping.[25] This relation is interesting since it gives

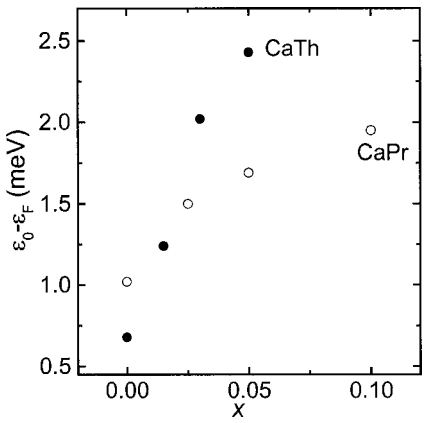

FIG. 5. $|\varepsilon_0-\varepsilon_F|$ vs x for the codoped samples. Solid symbols: Ca-Th. Open symbols: Ca-Pr.

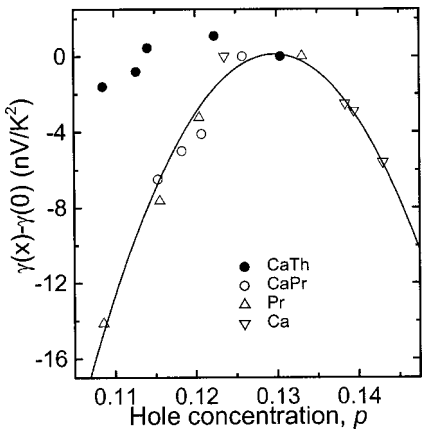

FIG. 6. Concentration dependence of the parameter γ from model 1. The hole concentration in the planes, p, was estimated from the thermopower and the general result of Ref. 15. Results for S of Ca-doped Nd-123 (Ref. 24) and Pr-doped Nd-123 (Ref. 25) are also shown. For Ca-Th-doped samples the parabolic relation between S and p breaks down as discussed in the text.

a further example of a parabolic relation between a material property of a high-T_c superconductor and the variation of charge. However, this result for $\gamma(p)$ is empirical and not understood in detail.

The present Ca-Pr-doped samples follow this trend, as illustrated in Fig. 6, indicating a decrease of (mobile) hole concentration with increasing Ca-Pr doping. For Ca-Th doping, on the other hand, this relation breaks down. This is apparently due to a breakdown of the relation between $S_{290\,K}$ and p. When p was estimated from bond valence sum calculations for Ca-Th-doped Nd-123,[20] it was found to increase with doping concentration x. On the other hand, since $S_{290\,K}$ increases with x, as shown in Fig. 2, the usual relation[15] between $S_{290\,K}$ and p indicates that p decreases with x. This is in contrast to Ca-Pr-doped Nd-123, where BVS estimates for p, although somewhat scattered, displayed a main trend of a decrease with increasing x.[19] As shown in Fig. 2, $S_{290\,K}$ increases with x also in this case. These results thus show another interesting difference between Ca-Pr and Ca-Th doping.

D. Results in model 2

In the description of $S(x,T)$ according to Eq. (2), results are obtained for the fraction of electron filling $F(x)$, and the two parameters $w_D(x)$ and $w_\sigma(x)$, referring to the bandwidths of the density of states and itinerant electrons, respectively. It was found that $F(x)$ remained almost constant for Ca-Pr doping and increased weakly for Ca-Th doping, with values about 0.52 for both dopings. The relative concentration dependence is illustrated in Fig. 7(a) on an expanded scale for F. These results support that charge filling in the bands remains approximately constant for both dopings.

w_D is shown in Fig. 7(b). It increases strongly with x for both dopings. The datum at $x=0.1$ for Ca-Th doping is shown within parentheses since it is at the solubility limit. Bandwidths of order 0.1 eV are in agreement with results by Gasumyants *et al.* for Y-123 samples doped by oxygen re-

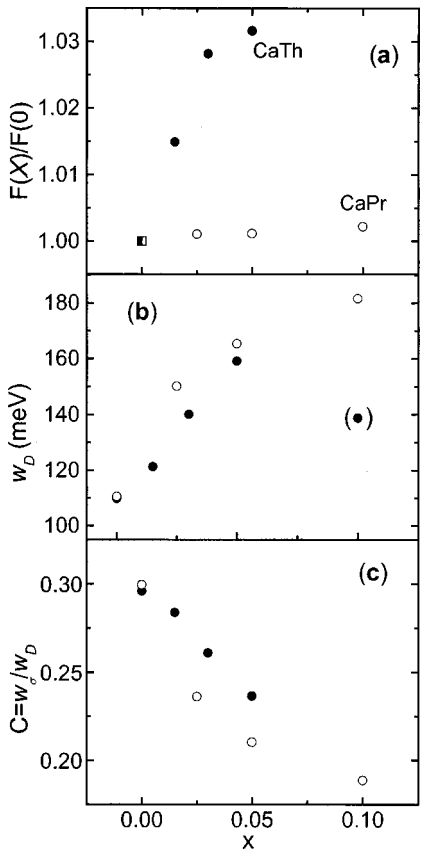

FIG. 7. Results from model 2. (a) The relative concentration dependence of the band filling $F(x)$ of Eq. (2). (b) Concentration dependence of the (density of states) band width. At $x=0.1$ the solubility limit in the orthorhombic phase is reached for Ca-Th doping, and this datum is shown within parentheses. (c) Concentration dependence of the localization parameter $C=w_\sigma/w_D$.

duction or addition of different $3d$ metals.[32] The strong increase of the bandwidths in Fig. 7(b) suggests that the density of states is reduced for both dopings. The itinerant electron bandwidth w_σ was found to increase somewhat with x for Ca-Th doping and to remain fairly constant for Ca-Pr doping as illustrated in Fig. 4. The development of these bandwidths with doping reflects a change of the metallic character, with the parameter $C=w_\sigma/w_D$ describing a tendency for localization. For both dopings, the increase of w_D [Fig. 7(b)] is stronger than the change of w_σ and C decreases as a function of doping concentration as seen in Fig. 7(c). The results thus suggest that band broadening mainly occurs in the localized parts of the bands.

IV. DISCUSSION

A. Trends in $S(x,T)$

Both models used to analyze $S(x,T)$ assume the existence of a narrow band in which the Fermi energy is located. Parameters of the models can therefore be qualitatively compared. Common trends in the doping dependence of such parameters give strengthened support for the outlines of a qualitative physical picture.

The effective bandwidth Γ in model 1 corresponds to the itinerant bandwidth w_σ in model 2. Here Γ was found to be of order 15 meV for both dopings, while w_σ is also similar for both dopings and about 35 meV. Quantitative agreement is thus poor. However, in semiempirical models it is rather the trends than the magnitudes of the parameters which are of physical relevance. The relative concentration dependences of w_σ and Γ are compared in Fig. 4. There is fair agreement between the results for the bandwidths in each of the two models. Γ and w_σ increase by about 15%–20% for Ca-Th doping, and for Ca-Pr doping they remain almost constant with the results in both models within $\pm 3\%$ in Fig. 4.

The tendency for localization as reflected in the parameter $C=w_\sigma/w_D$ in model 2 is related to the displacement of ε_F from the peak of the narrow band towards the localized part of the band in model 1. However, the development of the full bandwidth is not considered in model 1 and this comparison is rough. Nevertheless, from Figs. 5 and 7(c) it can be concluded that both models support an increased tendency towards localization for both dopings.

It is interesting to compare present charge-neutral doped systems with the results of Gasumyants *et al.*[32] for the thermopower of oxygen-depleted Y-123. This can conveniently be made by comparing the results over a range of similar changes of T_c. For the present alloys T_c has decreased by $\approx 20\%$ at $x=0.1$. A corresponding suppression in $YBa_2Cu_3O_{7-\delta}$ is found at $\delta \approx 0.3$,[33,34] and at this δ, w_D has increased by 70% over its value at optimal doping.[32] This is comparable to Ca-Pr doping where w_D from Fig. 7(b) increases by 65% when x increases from 0 to 0.1. Thus band broadening and a reduced density of states seem to be common important factors in the suppression of T_c for these two different alloy systems. On the other hand, the band filling factor F increases by 10% for Y-123 when the oxygen concentration is reduced to 6.7, while it increases by 0.2% for Ca-Pr doping from Fig. 7(a). This is characteristic for these different dopings where depletion of oxygen reduces charge while Ca-Pr doping conserves it. For Ca-Th the results are qualitatively similar to Ca-Pr doping, with a similar strong increase of w_D up to $x=0.05$ in Fig. 7(b) and a variation of F by a few percent in Fig. 7(a).

The analyses of both models give a consistent picture of Ca-Th and Ca-Pr dopings. An increased tendency for localization is found, and most results indicate that this tendency is stronger for Ca-Th than for Ca-Pr doping. The relative increase of the bandwidths $\Gamma(x)$ and $w_\sigma(x)$ with x is both stronger for Ca-Th doping (Fig. 4), and this is also the case for the energy distance between ε_0 and Fermi energy; i.e., ε_F moves faster towards the localized part of the band for Ca-Th doping (Fig. 5). The increase of $S_{290\,\mathrm{K}}$ with x is stronger for Ca-Th doping (Fig. 2), which empirically is in line with this picture. On the other hand, $T_{\max}(x)$ (Fig. 3) and the total bandwidth w_D [Fig. 7(b)] show a tendency for localization for both dopings, but the relative strengths of these trends cannot be clearly separated.

B. Depression of T_c in light of results from $S(T)$

Although the Ca-Th and Ca-Pr dopings in several aspects are similar, there are noteworthy differences as mentioned in

the Introduction. The most significant one in the present context is the strong increase of the room-temperature electrical resistivity ρ for Ca-Th-doped samples, compared with a much slower increase of ρ for Ca-Pr doping. In fact, in the approximation that the doping dependence of the resistivity measures the doping dependence of the disorder parameter $\hbar/\tau\varepsilon_F$, with τ the elastic scattering time, it was found that the depression of T_c could be qualitatively explained by quantum interference effects for Ca-Th doping, but not for Ca-Pr doping.[22] It might be possible that a larger resistivity for Ca-Th arises from an increased granularity. However, the present results for $S(x,T)$ confirm and supplement the picture of Ref. 22. The broadening of the bands and the displacement of the Fermi energy towards the localized bands qualitatively support a decrease of both τ and ε_F with increasing x, with a stronger effect for Ca-Th than for Ca-Pr doping.

Why then does electronic disorder develop faster for Ca-Th doping, and what causes the almost similarly strong depression of T_c for Ca-Pr doping? Tentative answers to these questions might be found along the following lines. It can be noted that Pr and Nd have comparable ionic masses, while Th is considerably heavier. One may therefore conjecture that Th produces a stronger perturbing potential with a larger increase of the electronic scattering rate. The alienation of Th in 123 compounds is also illustrated by the fact that it is the only one of the three doping elements Ca, Pr, and Th which does not easily enter into solid solutions as a single doping element.

For Pr doping it was found recently from neutron diffraction and calculations of BVS's that doping of only Pr in Nd-123 resulted in a suppression of mobile charge density.[35] Hybridization between Pr $4f$ and conduction electron band states may lead to such localization of charge carriers and depression of T_c, as inferred, e.g., from x-ray absorption fine structure in Pr-doped Y-123 (Ref. 36) and from magnetic properties of Pr doped into a large number of different rare-earth 123 compounds,[37] in both cases for larger Pr dopings than those presently studied. Localization may survive also in charge-neutral dopings. As mentioned, BVS results for the average hole density in the planes for Ca-Pr-doped Nd-123 showed a main trend of decreasing with increasing doping.[19] Using the present results for $S_{290\,K}$ to estimate the charge density, it can be inferred from the abscissa in Fig. 6 that p is similarly reduced for the present Ca_xPr_x samples up to $x=0.1$ as for $Nd_{1-x}Pr_x$-123 samples from Ref. 25 in the same range of x. Hence the localization tendency for Pr excess charge does not seem to be affected by codoping with Ca. For Ca-Pr doping we therefore conclude that in addition to an increased electronic disorder, the depression of T_c with doping is due to charge localization on Pr sites.

V. BRIEF SUMMARY

The normal-state thermoelectric power of $Nd_{1-2x}Ca_xM_xBa_2Cu_3O_{7-\delta}$ with $M=$ Pr or Th has been measured and analyzed in two different models, each one with three free parameters describing characteristic features of the band structure. Good descriptions of $S(T)$ were obtained in both models for each alloy system. A consistent doping concentration dependence of corresponding parameters was obtained in the two models. The bandwidths $\Gamma(x)$ and $w_\sigma(x)$ both increase for increasing Ca-Pr and Ca-Th doping, the Fermi energy is displaced towards the localized parts of the bands, and the ratio w_σ/w_D decreases with x. These changes are in general more prominent for Ca-Th doping, which together with a stronger increase of the electrical resistivity indicates that the localization tendency is driven by electronic disorder for this doping. For Ca-Pr doping the results suggest that in addition to a weaker disorder effect, mobile charge carriers localize for increasing doping concentration.

ACKNOWLEDGMENTS

Financial support by the Swedish Agencies Vetenskapsrådet and the SSF Oxide Consortium and from the Iranian Ministry of Science, Research, and Technology is gratefully acknowledged.

APPENDIX

In the model of Ref. 32, $S(T)$ is expressed in terms of the three parameters w_σ, w_D, and F as

$$S=-\frac{k_B}{e}\left\{\frac{w_\sigma^*}{\sinh w_\sigma^*}\left[e^{-\mu^*}+\cosh w_\sigma^*-\frac{1}{w_\sigma^*}(\cosh\mu^*+\cosh w_\sigma^*)\ln\frac{e^{\mu^*}+e^{w_\sigma^*}}{e^{\mu^*}+e^{-w_\sigma^*}}\right]-\mu^*\right\},$$

$$\mu^*=\frac{\mu}{k_BT}=\ln\frac{\sinh(Fw_D^*)}{\sinh[(1-F)w_D^*]},$$

$$w_D^*=\frac{w_D}{2k_BT},$$

and

$$w_\sigma^*=\frac{w_\sigma}{2k_BT}.$$

[1] J. R. Cooper, B. Alavi, L. W. Zhou, W. P. Beyeremann, and G. Grüner, Phys. Rev. B **35**, 9794 (1987).
[2] M. Sera and M. Sato, Physica C **185–189**, 1339 (1991).
[3] K. R. Krylov, A. I. Ponomarev, I. M. Tsidilkovski, V. I. Tsidilnitksi, V. G. Bazuev, V. L. Kozhevneikov, and S. M. Chesnitski, Phys. Lett. A **131**, 203 (1988).
[4] H. T. Trodahl and A. Mawdsley, Phys. Rev. B **36**, 8881 (1987).
[5] K. Matsuura, T. Wada, Y. Yeagashi, N. Suzuki, K. Kubo, H.

Yamauchi, and T. Tanaka, Physica C **185–189**, 1285 (1991).
[6] J. S. Zhou, J. P. Zhou, J. B. Goodenough, and J. T. MacDevitt, Phys. Rev. B **51**, 3250 (1995).
[7] C. Bernhard and J. L. Tallon, Phys. Rev. B **54**, 12 201 (1996).
[8] J. L. Tallon, J. R. Cooper, P. S. I. P. N. de Silva, G. V. M. Williams, and J. W. Loram, Phys. Rev. Lett. **75**, 4114 (1995).
[9] J. W. Cochrane, G. J. Russel, and D. N. Matthews, Physica C **232**, 89 (1994).
[10] G. V. M. Williams, M. Staines, J. L. Tallon, and R. Meinhold, Physica C **258**, 273 (1996).
[11] D. Mandrus, L. Forro, C. Kendziora, and L. Mihaly, Phys. Rev. B **44**, 2418 (1991).
[12] X. H. Chen, T. F. Li, M. Yu, K. Q. Ruan, C. Y. Wang, and L. Z. Cao, Physica C **290**, 317 (1997).
[13] R. Wang, H. Sekine, and H. Jin, Supercond. Sci. Technol. **9**, 529 (1996).
[14] M. Y. Choi and J. S. Kim, Phys. Rev. B **59**, 192 (1999).
[15] S. D. Obertelli, J. R. Cooper, and J. L. Tallon, Phys. Rev. B **46**, 14 928 (1992).
[16] C. N. R. Rao, T. V. Ramakrishnan, and N. Kumar, Physica C **165**, 183 (1990).
[17] K. Isawa, A. T. Okiwa-Yamamoto, M. Itoh, S. Adachi, and H. Yamauchi, Physica C **217**, 11 (1993).
[18] C. K. Subramaniam, M. Paranthaman, and A. B. Kaiser, Phys. Rev. B **51**, 1330 (1995).
[19] P. Lundqvist, C. Tengroth, Ö. Rapp, R. Tellgren, and Z. Hegedüs, Physica C **269**, 231 (1996).
[20] P. Lundqvist, Ö. Rapp, R. Tellgren, and I. Bryntse, Phys. Rev. B **56**, 2824 (1997).
[21] P. Lundqvist, Ö. Rapp, O. Hartmann, E. Karlsson, and R. Wäppling, Physica C **338**, 263 (2000).
[22] B. Lundqvist, P. Lundqvist, and Ö. Rapp, Phys. Rev. B **57**, 14 428 (1998).
[23] K. E. Johansson and P. E. Werner, J. Phys. E **13**, 1289 (1989).
[24] S. R. Ghorbani, M. Andersson, P. Lundqvist, M. Valldor, and Ö. Rapp, Physica C **339**, 245 (2000).
[25] S. R. Ghorbani, P. Lundqvist, M. Andersson, M. Valldor, and Ö. Rapp, Physica C **353**, 77 (2001).
[26] P. Lundqvist, P. Grahn, Ö. Rapp, and I. Bryntse, Physica C **289**, 137 (1997).
[27] J. B. Mandal, S. Keshri, P. Mandal, A. Poddar, A. N. Das, and B. Ghosh, Phys. Rev. B **46**, 11 840 (1992).
[28] S. Keshri, J. B. Mandal, P. Mandal, A. Poddar, A. N. Das, and B. Ghosh, Phys. Rev. B **47**, 9048 (1993).
[29] J. B. Mandal, A. N. Das, and B. Ghosh, J. Phys.: Condens. Matter **8**, 3047 (1996).
[30] L. Forro, J. Lukatela, and B. Keszei, Solid State Commun. **73**, 501 (1990).
[31] U. Gottwick, K. Gloos, S. Horn, F. Steglich, and N. Grewe, J. Magn. Magn. Mater. **47–48**, 536 (1985).
[32] V. E. Gasumyants, V. I. Kadanov, and E. V. Vladimirskaya, Physica C **248**, 255 (1995).
[33] R. J. Cava, A. W. Hewat, E. A. Hewat, B. Batlogg, M. Marezio, K. M. Rabe, J. J. Krajewski, W. F. Peck, and L. W. Rupp, Physica C **165**, 419 (1990).
[34] J. D. Jorgensen, B. W. Veal, A. P. Paulias, L. J. Nowicki, G. W. Crabtree, H. Claus, and W. K. Kwok, Phys. Rev. B **41**, 1863 (1990).
[35] S. R. Ghorbani, M. Andersson, and Ö. Rapp (unpublished).
[36] C. H. Booth, F. Bridges, J. B. Boyce, T. Claeson, Z. X. Zhao, and P. Cervantes, Phys. Rev. B **49**, 3432 (1994).
[37] W. Guan, Y. Xu, S. R. Sheen, Y. C. Chen, J. Y. T. Wei, H. F. Lai, M. K. Wu, and J. C. Ho, Phys. Rev. B **49**, 15 993 (1994).